

Luca Galantucci* and Michele Sciacca*

The wall effect in a plane counterflow channel

<https://doi.org/10.1515/jnet-2023-0123>

Received December 12, 2023; accepted February 17, 2024; published online March 19, 2024

Abstract: In this paper, we study the influence of the boundary conditions of the velocity fields in superfluid helium counterflow experiments. To make progress, we perform numerical simulations where we allow a slip velocity of the viscous component at the walls, and observe how this impacts on velocity fields and density profiles of distribution of quantized vortices. We conclude that the presence of a slip velocity at the walls generates a more homogeneous vortex distribution throughout the channel.

Keywords: liquid helium; quantized vortices; counterflow channel

PACS numbers: 47.37.+q; 67.40.Pm

1 Introduction

The full understanding of the behaviour of the low-temperature liquid phase of ^4He (hereafter referred to simply as helium II) is an open challenge: a model describing its behaviour at all the length scales [1]–[3] is in fact lacking, despite almost a century has passed since the observation of its superfluid properties. The name *superfluid* comes from its low viscosity, particularly observed when it flows in microchannels or in very thin layers. Superfluid helium finds application at CERN as refrigerator of the big magnets in the particle accelerators because of its extremely high thermal conductivity. Recent analytical studies have seen helium II used as refrigerator of hot spot energy dissipating devices immersed in a helium bath with and without mass flow [4]–[7]. These studies have been based on a thermodynamical approach and in particular by using the so-called one-fluid extended model of helium II [3].

In the last two decades, many investigations have focused in comparing turbulent flows in classical fluids and turbulent flows in helium II, as for instance in Ref. [8]–[11] where remarkable similarities between classical, homogeneous and isotropic turbulence and liquid helium turbulence have been established. These similarities arise as often helium II behaves as composed of two interpenetrating fluid components, according to the Landau's proposal: a viscous normal fluid (whose vorticity is unconstrained) and an inviscid superfluid (whose vorticity is confined to vortex lines of fixed circulation $\kappa = h/m$ with h the Planck's constant and m the mass of one helium atom). The classical experimental setup where helium II flows have been studied is thermal counterflow, which consists of a channel which is closed at one end, and open to the helium bath at the other end [12]–[18]. At the closed end, a resistor dissipates a known heat flux which is carried away by the normal fluid; the mass is conserved by the flowing of the superfluid component in the opposite direction towards the resistor; the resulting velocity difference between the two fluids is proportional to the applied heat flux. In terms of the usual one-fluid extended model, heat flux is the internal variable to add to the classical mean field velocity of the fluid. If this heat flux is higher than a (quite small) critical value, the superfluid component becomes

*Corresponding authors: Luca Galantucci, Istituto per le Applicazioni del Calcolo, Consiglio Nazionale delle Ricerche, via dei Taurini 19, 00185 Roma, Italy, E-mail: luca.galantucci@cnr.it; and Michele Sciacca, Dipartimento di Ingegneria, Università degli studi di Palermo, Viale delle Scienze, 90128 Palermo, Italy, E-mail: michele.sciacca@unipa.it

turbulent, forming a disordered tangle of quantized vortex lines (corresponding to the so-called quantum turbulence). Quantum turbulence is usually depicted as a tangle of vortices whose intensity is characterized by its vortex line density L (length of quantized vortex lines per unit volume), which can be determined either by measuring the attenuation of second sound or employing recently developed visualisation-based methods [19]–[22]. The vortex line density L is a function of the applied heat flux, temperature and the geometry of system. In the presence of walls Tough and collaborators derived the following relation

$$L^{1/2}D = 1.03\gamma_0 \frac{\rho}{\rho_s} \langle v_n \rangle h_D - 1.48\beta \quad (I.1)$$

where D is the channel width, h_D is the hydraulic diameter, $\langle v_n \rangle = \frac{\bar{q}}{\rho_s T}$ is the average normal fluid velocity, T being the absolute temperature, \bar{q} the applied heat flux, S the specific entropy, ρ_n the normal density, ρ_s the superfluid density and $\rho = \rho_n + \rho_s$ the total density. The coefficients γ_0 and β have been determined experimentally by Tough's group [16]–[18].

Two distinct regimes have been observed in counterflow experiments, usually referred to as TI and TII. Two explanations are proposed in literature: the first, by Melotte and Barenghi [23], shows that the normal component is unstable in the TII regime and hence the normal component may undergo a laminar-turbulent transition when switching from the TI regime to the TII regime; instead, the second, by Jou and Mongiovi, asserts that the TII regime is caused by the loss of a strong polarization of the vortex tangle existing in the TI regime. It is important to emphasize that the two distinct regimes have only been observed in small enough channels [18], while in large channel only one regime, TII, is observed [24].

This unsolved puzzle has motivated experimental attempts to directly visualize the flow of helium II and the quantised vortices. The most employed experimental technique to achieve this aim is the Particle Tracking Velocimetry (PTV) of hydrogen and/or deuterium flakes [25]–[27] which is used to visualize quantum vortex reconnections [28] or to determine the statistics of the turbulent superfluid [29], [30]. On the other hand, laser-induced fluorescence of metastable helium molecules is used in Ref. [31], [32] to directly image the profile of the normal component in order to determine whether, at sufficiently large heat currents, the normal fluid flow undergoes a laminar-turbulent transition. In [33] we computed the velocity profiles of normal fluid and superfluid components and the distribution of the quantized vortices in a two-dimensional wall-bounded flow, highlighting the fundamental role played by the mutual friction force. In almost all previously cited studies the normal component is assumed to behave as a classical fluid (according to the two-fluid model) with no-slip condition on the boundaries, while the superfluid component is free to slip on the latter (only the wall-normal velocity component is imposed to zero).

For an exhaustive overview, most of the numerical simulation of superfluid turbulence in literature are based on determining the superfluid vortex tangle in the presence of a prescribed normal fluid, without considering the back reaction of the vortex lines on the normal fluid. In all these models normal component is assumed to be a classical viscous fluid in open or periodic domains, avoiding the difficulty of the boundaries. There are only a few numerical studies which have considered the influence of the walls, such as [33], [34]. Other papers have determined the effects of a prescribed superfluid tangle on the normal fluid [23] neglecting to model the coupling of superfluid and normal fluid. From the experimental point of view, the impact of solid boundaries on the near-wall flow region has been investigated employing Particle Image Velocimetry (PIV) [35] and PTV [19]–[21].

In this paper we use the two dimensional model proposed in [33], where the two components are fully coupled (the normal fluid affects the superfluid and vice versa via a nonlinear mutual friction term), and we study the role of boundaries removing the classical constraint of no-slip boundary condition for the normal velocity. This model is two-dimensional hence vortex loops in a three-dimensional channel correspond to vortex points in our two-dimensional channel.

There is a further mathematical model, the so-called one-fluid extended model, proposed by using the Extended Thermodynamics, which considers heat flux as a further field for describing some peculiarities of helium II [3], instead of assuming that helium II is a mixture of two fluids. The two velocities of the normal and superfluid components, \mathbf{v}_n and \mathbf{v}_s , may be related to the velocity and heat flux \mathbf{v} and \mathbf{q} in the one-fluid model, by the following:

$$\mathbf{v}_n = \mathbf{v} + \frac{1}{\rho(S - S_s)T} \mathbf{q}, \quad \mathbf{v}_s = \mathbf{v} - \frac{S - S_s}{\zeta} \mathbf{q}. \quad (\text{I.2})$$

where $\zeta = \rho \frac{\rho_s}{\rho_n} TS^2$ and S_s is the specific entropy associated to the superfluid component. In Ref. [36], [37] it was experimentally found that this amount is very small and it is within 3 % of the whole entropy at temperature higher than 1.27 K but less than T_λ . Putterman asserted that the statement that the superfluid component does not carry entropy has not been demonstrated theoretically, but it is a further hypothesis [38]. Further theoretical studies considered the presence of an entropy for the superfluid component [3], [39], [40], and in [41] it was suggested how to measure the small entropy carried by the superfluid component using the one-fluid extended model. Note that if $S_s = 0$, as usual, the fields \mathbf{v}_n and \mathbf{v}_s coincide with those in the two-fluid model.

In terms of the two-fluid model, the normal component is a viscous fluid, hence it is logical to take $\mathbf{v}_n|_{\text{wall}} = 0$ on the wall and the slip condition for the superfluid components. In terms of the one-fluid model however, the main fields would be the heat flux \mathbf{q} and the velocity \mathbf{v} . In phonon hydrodynamics the collision of phonons against the walls may play an important role if the mean-free path of these phonons ℓ_m is comparable to the size of the system (*e.g.* the channel width D). Indeed, the heat flux on the wall \mathbf{q}_{wall} satisfies the following relation

$$\mathbf{q}_{\text{wall}} = -C\ell_m \left(\frac{\partial \mathbf{q}}{\partial \xi} \right)_{\text{wall}} \quad (\text{I.3})$$

where C is a constant which depend on the material and geometry, and ξ is the outward-pointing variable. This relation was used for the first time in [42] for taking into account of the contribution of phonon-boundary scattering (boundary contribution on the flowing heat flux) in the phonon hydrodynamics in nanosystems and it was borrowed from the microfluidics [43], [44]. It is expected that it is valid in the ballistic regime in helium II, namely when $T < 0.7$ K [45]. The existence of a slip heat flux at the boundaries of the channel implies that also the flow of the normal component might be non-vanishing at the boundaries. In the present study, we discuss the implications if such slip flow of the normal component at the boundaries also exists when $T > 0.7$ K, *i.e.* in the hydrodynamic regime, possibly triggering an interesting debate on the effects of the walls in superfluid helium flows. To assess the implications of normal flow at the boundaries, we have performed a numerical experiment employing the model proposed in [33], assuming a slip condition for the normal component \mathbf{v}_n .

The paper is organized as follow: in Section 2 the mathematical model is recalled and revised according to the new condition on the boundaries; Section 3 is devoted to the results of the numerical experiments with the parameters used, and finally, the last Section is for the Conclusions of the paper.

2 The mathematical model

In this section we follow the general lines of the paper [33], which considers an infinite two-dimensional channel along x of width D along y with $-D/2 \leq y \leq D/2$ and periodic boundary conditions imposed at $x = 0$ and $x = L_x$. Our numerical experiments are applied to a counterflow channel in terms of the two-fluid model. More details about the numerical code can be found in [33], [46].

The dynamics of the normal component is given by equations

$$\nabla \cdot \mathbf{v}_n = 0 \quad (\text{II.4})$$

$$\frac{\partial \mathbf{v}_n}{\partial t} + (\mathbf{v}_n \cdot \nabla) \mathbf{v}_n = -\frac{1}{\rho} \nabla p - \frac{\rho_s}{\rho_n} S \nabla T + \nu \nabla^2 \mathbf{v}_n - \frac{\rho_s}{2\rho} \nabla (\mathbf{v}_n - \mathbf{v}_s)^2 + \frac{1}{\rho_n} \tilde{\mathbf{F}}_{ns}, \quad (\text{II.5})$$

where the mutual friction term $\tilde{\mathbf{F}}_{ns}$ has been considered because of the interaction between the normal component and the quantized vortices [47].

The Cauchy–Dirichlet problem associated to (II.4) and (II.5) is:

$$\begin{aligned} \mathbf{v}_n(x, \pm D/2) &= (c, 0) \quad \forall t \\ \mathbf{v}_n(x, y)|_{t=0} &= (-V_{n0} [1 - (2y/D)^2] + c, 0) \end{aligned} \quad (\text{II.6})$$

together with the counterflow condition

$$\rho_n \bar{\mathbf{v}}_n + \rho_s (\bar{\mathbf{v}}_{s0} + \bar{\mathbf{v}}_{si}) = 0, \quad (\text{II.7})$$

where $\bar{\cdot}$ indicates channel-averaged quantities, \mathbf{v}_{s0} is the constant imposed superflow enforcing the counterflow condition and \mathbf{v}_{si} is the superfluid velocity induced by the vortices. The constant c in (II.6) takes into account the partial slip condition of the normal component along the wall of the channel. We choose two distinct pairs (c, V_{n0}) such that the flow rate (and hence the applied heat flux and the number of vortices) is constant.

The calculation will regard the dynamics of the vortex points over the channel, ideally describing the dynamics of the vortex lines in three-dimensions, and the dynamical equation for the normal component. The velocity field of the superfluid component is obtained by means of the superfluid field induced by all vortex points and by the counterflow condition (II.7).

Quantized vortices in a two-dimensional channel are described by N vortex-points of circulation κ (half of them have positive circulation and half have negative circulation) in the plane with $\mathbf{r}_j(t) = (x_j(t), y_j(t))$, where $j = 1, \dots, N$, which satisfies the following equation proposed by Schwarz [48]

$$\begin{aligned} \frac{d\mathbf{r}_j}{dt} &= \mathbf{v}_{s0}(\mathbf{r}_j, t) + \mathbf{v}_{si}(\mathbf{r}_j, t) + \alpha \mathbf{s}'_j \times (\mathbf{v}_n(\mathbf{r}_j, t) - \mathbf{v}_{s0}(\mathbf{r}_j, t) - \mathbf{v}_{si}(\mathbf{r}_j, t)) \\ &\quad + \alpha' (\mathbf{v}_n(\mathbf{r}_j, t) - \mathbf{v}_{s0}(\mathbf{r}_j, t) - \mathbf{v}_{si}(\mathbf{r}_j, t)) \end{aligned} \quad (\text{II.8})$$

where \mathbf{s}'_j is the unit vector along vortex j (in the positive z direction when the quantum of circulation is $\Gamma_j = \kappa$ and in the negative z direction when $\Gamma_j = -\kappa$), α and α' are the temperature-dependent mutual friction coefficients [49], the field $\mathbf{v}_n(\mathbf{r}_j, t)$ is the normal fluid velocity at position \mathbf{r}_j , $\mathbf{v}_{si}(\mathbf{r}_j, t) = \sum_{k=1 \dots N} \mathbf{v}_{si,k}(\mathbf{r}_j, t)$ is the superfluid velocity field induced by all N vortex-points at \mathbf{r}_j and $\mathbf{v}_{s0} = (u_{s0x}, 0)$ is the superfluid flow which enforces the counterflow condition $\rho_n \bar{\mathbf{v}}_n + \rho_s (\bar{\mathbf{v}}_{s0} + \bar{\mathbf{v}}_{si}) = 0$ at each channel cross-section (further details in [33]). Hence, superfluid velocity \mathbf{v}_s in a point \mathbf{r} is given by the sum of the contribution of each vortex point $\mathbf{v}_{si}(\mathbf{r})$ and the constant contribution \mathbf{v}_{s0} , satisfying the counterflow condition $\rho_n \bar{\mathbf{v}}_n + \rho_s (\bar{\mathbf{v}}_{s0} + \bar{\mathbf{v}}_{si}) = 0$.

We choose the same algorithm used in [33] for the creation and the destruction of vortex points, namely the “numerical vortex reconnection” which has been described, tested and employed in our papers [33], [34], [46], [50], [51]. A couple of vortex points is removed when the distance between the two vortex points of opposite circulation becomes smaller than a critical value ϵ_1 or when the distance between a vortex point and a channel wall is less than $0.5\epsilon_1$. They are then re-inserted randomly in the channel (more details in Ref. [33] and in the Supplementary Material of Ref. [34]).

The dynamics of the normal fluid is studied by applying the vorticity-stream function formulation to equations (II.4) and (II.5)

$$\nabla^2 \Psi = -\omega_n, \quad (\text{II.9})$$

$$\frac{\partial \omega_n}{\partial t} + \frac{\partial \Psi}{\partial y} \frac{\partial \omega_n}{\partial x} - \frac{\partial \Psi}{\partial x} \frac{\partial \omega_n}{\partial y} = v_n \nabla^2 \omega_n + \frac{1}{\rho_n} \left(\frac{\partial \tilde{F}^y}{\partial x} - \frac{\partial \tilde{F}^x}{\partial y} \right) \quad (\text{II.10})$$

where the stream function Ψ and the normal vorticity ω_n are defined by $\mathbf{v}_n = \left(\frac{\partial \Psi}{\partial y}, -\frac{\partial \Psi}{\partial x} \right)$ and $\omega_n = \nabla \times \mathbf{v}_n$ respectively, and the mutual friction force $\tilde{\mathbf{F}}_{ns} = (\tilde{F}^x, \tilde{F}^y)$ is computed employing the coarse-grained theoretical framework proposed by Hall and Vinen [52], at length scales larger than the average inter-vortex spacing ℓ . Thus, we distinguish between the fine $(\Delta x, \Delta y)$ grid where \mathbf{v}_n is numerically determined, and the coarser $(\Delta X, \Delta Y)$ grid on which we define the mutual friction $\tilde{\mathbf{F}}_{ns}$ given by Hall and Vinen:

$$\tilde{\mathbf{F}}_{ns} = \alpha \rho_s \hat{\tilde{\omega}}_s \times [\tilde{\omega}_s \times (\tilde{\mathbf{v}}_n - \tilde{\mathbf{v}}_n)] + \alpha' \rho_s \tilde{\omega}_s \times (\tilde{\mathbf{v}}_n - \tilde{\mathbf{v}}_n), \quad (\text{II.11})$$

where $\tilde{\cdot}$ symbols indicate coarse-grained averaged quantities, namely the fields are averaged over coarse grid-cells. For the evaluation of the mutual friction force $\tilde{\mathbf{F}}_{ns}$ on the coarse grid, we interpolate it on the finer grid via a two-dimensional bicubic convolution kernel [53].

In Tables 1 and 2 we report a complete list of parameters and physical relevant quantities employed in our simulations, some of them expressed in terms of the units of length, velocity and time, respectively: $\delta_c = D/2 = 1.0 \times 10^{-1}$ cm, $u_c = \kappa/(2\pi\delta_c) = 1.59 \times 10^{-3}$ cm/s, $t_c = \delta_c/u_c = 62.79$ s. All the quantities are dimensionless, unless otherwise stated. The parameters employed in the present simulations, in particular the channel width D , the average inter-vortex spacing $\ell = L^{-1/2}$ (following by the number of vortex points N) and the normal fluid volume flow-rate (imposed by the parameters V_{n0} and c) are chosen to make at least qualitative comparisons with the experimental setup used by the Prague's group.

We use also the tangle polarization \mathbf{p} , namely the average value of the unit vector \mathbf{s}' tangent to the vortex line on the small volume Λ [54]–[58]

$$\mathbf{p} = \langle \mathbf{s}' \rangle = \frac{1}{\Lambda L} \int \mathbf{s}' d\xi = \frac{\nabla \times \mathbf{v}_s}{\kappa L} \quad (\text{II.12})$$

which in a two-dimensional channel gives information about the distribution of the polarization all over the channel.

3 Results

In this section we apply the mathematical model proposed in the previous section to helium II counterflows with parameters reported in Tables 1 and 2. These parameters almost coincide with those used in [33] exception made for the slip condition for the normal component arising from thermodynamical considerations on the basis of the one-fluid extended model.

To take into account of the slip condition in (II.6), we have assumed that the wall-parallel component of the normal fluid velocity at the walls is equal to the constant c , which we choose together with V_{n0} in order to maintain the flow rate of the normal fluid unchanged with respect to the numerical simulations performed in [33]. The two different values of the constant c employed in the present work are listed in Table 1 and the results corresponding to the case $c = 0$ [33] are reported in Figure 1 for completeness.

3.1 The case $c^A = -100.0$

In Figure 2 the results of the first numerical experiments with $c = c^A = -100.0$ is reported. The profile of the normal and superfluid component (left) is still parabolic-like but flatter than those found in Ref. [33] because of

Table 1: Physical and numerical parameters employed in the simulations in dimensionless units.

$D = 2$		$T = 1.7$ K
$L_x = 6$		$\rho_s/\rho_n = 3.373$
$N = 1876$		$\Delta t_v = 7.5 \times 10^{-6}$
$n = 156.3$		$\epsilon_1 = 2.5 \times 10^{-3}$
$V_{n0}^A = 403.19$		$c^A = -100.0$
$V_{n0}^B = 178.19$		$c^B = -250.0$

Table 2: Number of grid-points and spacings in dimensionless units of the grids employed in the simulations.

Fine grid		Coarse grid	
n_x	192	N_x	48
n_y	64	N_y	16
Δx	3.125×10^{-2}	ΔX	0.125
Δy	3.125×10^{-2}	ΔY	0.125

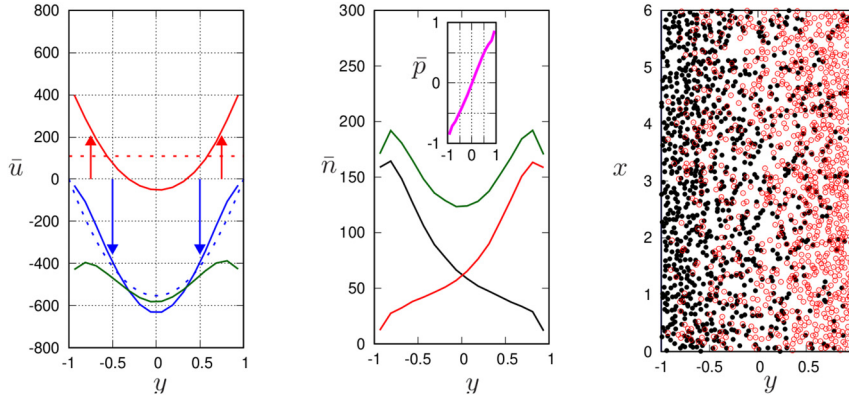


Figure 1: Left: Plot of the velocity profiles of the normal (blue) and superfluid (red) component, and of the relative velocity \mathbf{v}_{ns} (green line). Blue (red) arrows indicate the flow direction of the normal fluid (superfluid) flow; Middle: plot of the positive vortex density (red), negative vortex density (black), vortex density (green), and of the polarization vector (pink line in the little box); Right: distribution of the vortex points in the steady state: positive (red) and negative (black). The results refer to the case $c = 0$ [33].

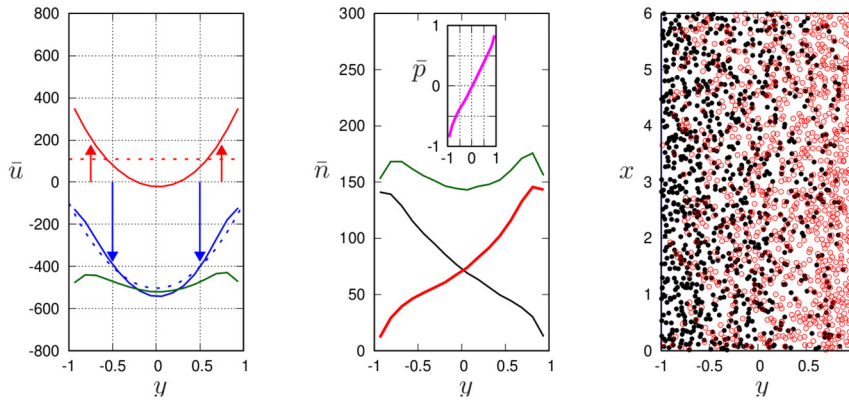


Figure 2: Left: Plot of the velocity profiles of the normal (blue) and superfluid (red) component, and of the relative velocity \mathbf{v}_{ns} (green line). Blue (red) arrows indicate the flow direction of the normal fluid (superfluid) flow; Middle: plot of the positive vortex density (red), negative vortex density (black), vortex density (green), and of the polarization vector (pink line in the little box); Right: distribution of the vortex points in the steady state: positive (red) and negative (black). The results refer to the case $c = c^A = -100.0$.

the sliding conditions on the wall. In the same figure we have also reported the profile of the relative velocity \mathbf{v}_{ns} (green line), which is proportional to the heat flux because of the relation $\mathbf{q} = \rho_s S T \mathbf{v}_{ns}$. In Guo's experiments [31], [32] the metastable helium molecules, carried by the normal component, show an almost flat profile. Thus, the results of the present paper are more exhaustive than those found in our previous numerical experiments.

In Figure 2 (middle and right) we plot the distribution of the positive and negative vortices as well as the polarization vector. From a direct comparison with our previous paper, we do not note remarkable difference in terms of vortex distribution.

3.2 The case $c^B = -250.0$

In this section we report the results of the numerical experiments assuming a stronger slip condition for the normal components, $c = c^B = -250.0$. In Figure 3 we report the same plots as in Figure 2 for the sake of direct comparison with the lower slipping condition for the normal component.

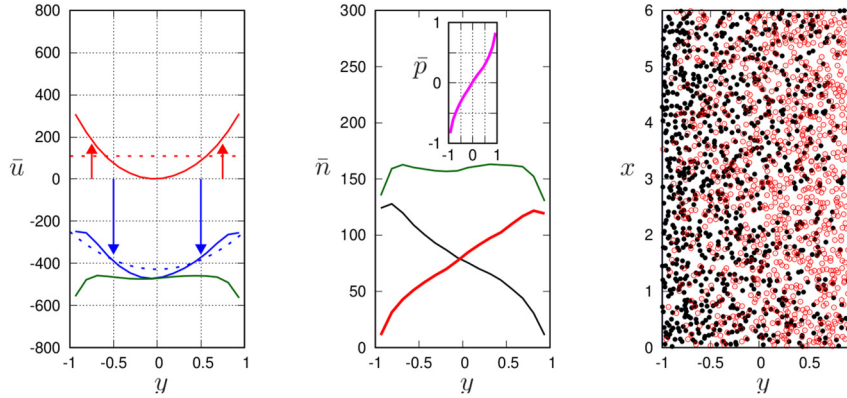


Figure 3: Left: Plot of the velocity profiles of the normal (blue) and superfluid (red) component, and of the relative velocity \mathbf{v}_{ns} (green line). Blue (red) arrows indicate the flow direction of the normal fluid (superfluid) flow; Middle: plot of the positive vortex density (red), negative vortex density (black), vortex density (green), and of the polarization vector (pink line in the little box); Right: distribution of the vortex points in the steady state: Positive (red) and negative (black). The results refer to the case $c = c^B = -250.0$.

As shown in the left figure, the profile of the normal component is more flattened than the previous situations and it would describe better the behaviour of the metastable helium molecules in the experiments [31] in terms of the two-fluid model. The overall distribution of the vortices throughout the channel is more homogeneous: the vortex density distribution shows in fact a flat profile in Figure 3 (middle).

4 Conclusions

In this paper we have performed further numerical experiments for better understanding the experiments by Guo's group [31], [32], with particular emphasis to the contribution of the walls. The idea comes from the new frontiers of heat transport in nanosystems, which uses arguments of the non equilibrium thermodynamics when the Fourier's law ceases to be valid, as in helium II.

Indeed, in the ballistic regime ($T < 0.7$ K) the heat flux at the boundary might be non vanishing (as determined by relation (I.3)), implying the potential existence of a slip normal fluid velocity at the boundary. In our work, we explore the implications arising when considering the possibility that such non vanishing normal fluid flow at the boundaries also occurs at higher temperatures where experiments are performed. For this purpose we have imposed a non-zero streamwise normal fluid velocity c at the solid boundaries and compared the results obtained with our previous numerical investigations.

In Figures 2 and 3 we have reported the results of our numerical simulations, where the slip normal velocities are $c^A = -100.0$ and $c^B = -250.0$ respectively, while in Figure 1 we report the results obtained with no-slip boundary conditions imposed on the normal fluid flow, already described in literature [33]. More precisely, in the left panel of Figures 1–3, we have reported the velocity profiles of the normal (blue) and superfluid (red) components with the normal component flowing in the same direction of the heat flux (downwards) and the superfluid component flowing in the opposite direction (upwards) in order to satisfy the counterflow condition of zero net mass flow. The dashed lines refer to the initial condition of the two velocity profiles while the green line is the counterflow velocity \mathbf{v}_{ns} , proportional to the heat flux. In the middle panel of Figures 1–3 we plot the wall-normal profile of the vortex points density $n(y)$ (number of vortices per unit area): the red line refers to vortices with positive circulation (counterclockwise), the black line to vortices with negative circulation (clockwise) and the green line refers to the total vortex density. The pink line refers to the profile of the polarization of tangle (II.12). In the left panel of Figures 1–3 we show a snapshot of the vortex distribution in the channel in the steady state: positive vortices (red) move towards the right boundary, whereas negative vortices (black) move towards the left; both positive and negative vortices move upwards, following the superfluid component.

In Guo's experiments the metastable helium molecules show an almost flat profile. From a direct comparison between the results found in [33] (Figure 1) and those shown in Figures 2 and 3 we see that the presence of the slip condition for the normal component, especially the highest c^B , leads to a flatter profile for the normal component, even though it is still parabolic-like. This would mean that the velocity of the normal component is not properly zero on the wall and that the assumption of no-slip condition probably does not well describe the behaviour of helium II on the wall. We hope that the results of the present paper open the debate about the behaviour of superfluid helium next to the wall, leading to further studies and experiments.

There is a further interpretation about the results found here, when compared to Guo's experiments, which may be useful for the debate. In our paper we have used the usual interpretation of superfluid helium, that it is composed by the two undistinguished components: normal and superfluid. Even though it is well-known that it is a toy-model proposed by Landau almost a century ago, it is well used for describing the experiments of helium II.

Let's just for a while forget this model, and uses the so-called one-fluid extended model, where the mean fields are the mean velocity \mathbf{v} and heat flux \mathbf{q} , among others. According to the relation $\mathbf{q} = \rho_s ST \mathbf{v}_{ns}$, the heat flux is proportional to the counterflow velocity \mathbf{v}_{ns} , which is shown in Figures 2 and 3. If the heat flux is essentially the heat carried away by the phonons and rotons, which are the particles interacting with the metastable helium molecules in Guo's experiments, then the profiles to compare with those shown in Guo's papers are the green curves in Figures 2 and 3, namely those of the counterflow velocity, proportional to \mathbf{q} . In this spirit, the results obtained in our work are consistent with the experimental findings as the observed profile of the metastable helium molecules and the heat flux profile calculated in the present study are both flat.

Acknowledgments: M.S. acknowledges the financial support of the Istituto Nazionale di Alta Matematica (GNFM–Gruppo Nazionale della Fisica Matematica) and of the Università degli studi di Palermo.

Research ethics: Not applicable.

Author contributions: The authors have accepted responsibility for the entire content of this manuscript and approved its submission.

Competing interests: The authors state no competing interests.

Research funding: This paper is partially supported by the PNRR project ECS00000022 “SiciliAn MicronanOTech Research And innovation CEntER (SAMOTHRACE)” and the project PRJ-1020 “Innovative models of Heat transFER in additive mAnufacturing processes via powder bed fusion with short lengTh laser source (IHEAT)”.

Data availability: Not applicable.

References

- [1] R. J. Donnelly, “An introduction to experiments on superfluid turbulence,” in *Quantized Vortex Dynamics and Superfluid Turbulence*, Springer, 2001, pp. 17–35.
- [2] C. F. Barenghi, R. J. Donnelly, and W. F. Vinen, *Quantized Vortex Dynamics and Superfluid Turbulence*, Berlin, Springer, 2001.
- [3] M. S. Mongioli, D. Jou, and M. Sciacca, “Non-equilibrium thermodynamics, heat transport and thermal waves in laminar and turbulent superfluid helium,” *Phys. Rep.*, vol. 726, no. 6, pp. 1–71, 2018.
- [4] M. Sciacca, A. Sellitto, L. Galantucci, and D. Jou, “Refrigeration of an array of cylindrical nanosystems by superfluid helium counterflow,” *Int. J. Heat Mass Transfer*, vol. 104, pp. 584–594, 2017.
- [5] D. Jou, L. Galantucci, and M. Sciacca, “Refrigeration of an array of cylindrical nanosystems by flowing superfluid helium,” *J. Low Temp. Phys.*, vol. 187, nos. 5–6, pp. 602–610, 2017.
- [6] M. Sciacca, A. Sellitto, L. Galantucci, and D. Jou, “Thermodynamics of computation and linear stability limits of superfluid refrigeration of a model computing array,” *Z. Angew. Math. Phys.*, vol. 70, no. 4, pp. 1–15, 2019.
- [7] D. Jou, M. Sciacca, A. Sellitto, and L. Galantucci, “Refrigeration bound of heat-producing cylinders by superfluid helium,” in *Atti della Accademia Peloritana dei Pericolanti-Classe di Scienze Fisiche, Matematiche e Naturali*, vol. 97, Messina, Accademia Peloritana dei Pericolanti, 2019, p. 12.
- [8] L. Skrbek and K. Sreenivasan, “Developed quantum turbulence and its decay,” *Phys. Fluids*, vol. 24, no. 1, p. 011301, 2012.
- [9] S. K. Nemirovskii, “Quantum turbulence: theoretical and numerical problems,” *Phys. Rep.*, vol. 524, no. 3, pp. 85–202, 2013.
- [10] S. Nemirovskii, “Modeling of classical turbulence by quantized vortices,” *J. Eng. Thermophys.*, vol. 26, no. 4, pp. 476–484, 2017.
- [11] C. F. Barenghi, L. Skrbek, and K. R. Sreenivasan, *Quantum Turbulence*, Cambridge, Cambridge University Press, 2023.

- [12] W. Vinen, “Mutual friction in a heat current in liquid helium II. I. Experiments on steady heat current,” *Proc. R. Soc. London, A*, vol. 240, no. 1220, pp. 114–127, 1957.
- [13] W. Vinen, “Mutual friction in a heat current in liquid helium II. II. Experiments on transient effects,” *Proc. R. Soc. London, A*, vol. 240, no. 1220, pp. 128–143, 1957.
- [14] D. Brewer and D. Edwards, “Heat conduction by liquid helium II in capillary tubes ii. measurements of the pressure gradient,” *Philos. Mag.*, vol. 6, no. 69, pp. 1173–1181, 1961.
- [15] R. Childers and J. Tough, “Helium II thermal counterflow: temperature-and pressure-difference data and analysis in terms of the Vinen theory,” *Phys. Rev. B*, vol. 13, no. 3, pp. 1040–1055, 1976.
- [16] D. R. Ladner and J. T. Tough, “Temperature and velocity dependence of superfluid turbulence,” *Phys. Rev. B*, vol. 20, no. 7, pp. 2690–2702, 1979.
- [17] K. P. Martin and J. T. Tough, “Evolution of superfluid turbulence in thermal counterflow,” *Phys. Rev. B*, vol. 27, no. 5, pp. 2788–2799, 1983.
- [18] J. Tough, “Superfluid turbulence,” in *Progress of Low Temperature Physics*, vol. VIII, D. Brewer, ed., North Holland, 1982, pp. 133–219.
- [19] M. La Mantia, “Particle dynamics in wall-bounded thermal counterflow of superfluid helium,” *Phys. Fluids*, vol. 29, no. 6, p. 065102, 2017.
- [20] P. Svancara, *et al.*, “Visualization study of thermal counterflow of superfluid helium in the proximity of the heat source by using solid deuterium hydride particles,” *Phys. Rev. Fluids*, vol. 997, no. 11, p. 064512, 2018.
- [21] P. Hrubcova, *et al.*, “Vorticity enhancement in thermal counterflow of superfluid helium,” *Phys. Rev. B*, vol. 3, no. 6, p. 114701, 2018.
- [22] W. Kubo and Y. Tsuji, “Statistical properties of small particle trajectories in a fully developed turbulent state in He-II,” *J. Low Temp. Phys.*, vol. 196, no. 15, pp. 170–176, 2019.
- [23] D. J. Melotte and C. F. Barenghi, “Transition to normal fluid turbulence in helium II,” *Phys. Rev. Lett.*, vol. 80, no. 19, pp. 4181–4184, 1998.
- [24] M. La Mantia, “Particle trajectories in thermal counterflow of superfluid helium in a wide channel of square cross section,” *Phys. Fluids*, vol. 28, no. 2, p. 024102, 2016.
- [25] G. P. Bewley, D. P. Lathrop, and K. R. Sreenivasan, “Visualization of quantized vortices,” *Nature*, vol. 441, no. 31, p. 588, 2006.
- [26] T. Chagovets and S. Van Sciver, “A study of thermal counterflow using particle tracking velocimetry,” *Phys. Fluids*, vol. 23, no. 10, p. 107102, 2011.
- [27] M. La Mantia, T. Chagovets, M. Rotter, and L. Skrbek, “Testing the performance of a cryogenic visualization system on thermal counterflow by using hydrogen and deuterium solid tracers,” *Rev. Sci. Instrum.*, vol. 83, no. 5, p. 055109, 2012.
- [28] G. P. Bewley, M. S. Paoletti, K. R. Sreenivasan, and D. P. Lathrop, “Characterization of reconnecting vortices in superfluid helium,” *Proc. Natl. Acad. Sci. U. S. A.*, vol. 105, no. 37, pp. 13707–13710, 2008.
- [29] M. S. Paoletti, M. E. Fisher, K. R. Sreenivasan, and D. P. Lathrop, “Velocity statistics distinguish quantum turbulence from classical turbulence,” *Phys. Rev. Lett.*, vol. 101, no. 15, p. 154501, 2008.
- [30] M. La Mantia, D. Duda, M. Rotter, and L. Skrbek, “Lagrangian accelerations of particles in superfluid turbulence,” *J. Fluid Mech.*, vol. 717, no. 25, p. R9, 2013.
- [31] W. Guo, S. B. Cahn, J. A. Nikkel, W. F. Vinen, and D. N. McKinsey, “Visualization study of counterflow in superfluid ^4He using metastable helium molecules,” *Phys. Rev. Lett.*, vol. 105, no. 4, p. 045301, 2010.
- [32] A. Marakov, *et al.*, “Visualization of the normal-fluid turbulence in counterflowing superfluid He^4 ,” *Phys. Rev. B*, vol. 91, no. 9, p. 094503, 2015.
- [33] L. Galantucci, M. Sciacca, and C. F. Barenghi, “Coupled normal fluid and superfluid profiles of turbulent helium II in channels,” *Phys. Rev. B*, vol. 92, no. 17, p. 174530, 2015.
- [34] L. Galantucci, M. Sciacca, and C. F. Barenghi, “Large-scale normal fluid circulation in helium superflows,” *Phys. Rev. B*, vol. 95, no. 1, p. 014509, 2017.
- [35] T. Xu and S. W. Van Sciver, “Particle Image Velocimetry measurements of the velocity profile in He II forced flow,” *Phys. Fluids*, vol. 19, no. 7, p. 071703, 2007.
- [36] A. Singaas and G. Ahalersz, “Entropy of He II from 1.6 K to the λ line,” *Phys. Rev. B*, vol. 29, no. 9, pp. 4951–4960, 1984.
- [37] F. I. Glick and J. H. Wernitz, “Entropy of the superfluid component of helium,” *Phys. Rev.*, vol. 178, no. 1, pp. 314–319, 1969.
- [38] S. Putterman, *Superfluid Hydrodynamics*, Amsterdam, North-Holland Publishing Co., 1974.
- [39] T. Fliessbach, “A model for the λ -transition of helium,” *Il Nuovo Cimento D*, vol. 13, pp. 211–231, 1991.
- [40] R. Schäfer and T. Fliessbach, “The two-fluid model with superfluid entropy,” *Il Nuovo Cimento D*, vol. 16, pp. 373–390, 1994.
- [41] M. S. Mongiovi, “Proposed measurements of the small entropy carried by the superfluid component in liquid helium II,” *Phys. Rev. B*, vol. 63, no. 1, p. 012501, 2000.
- [42] F. X. Alvarez, D. Jou, and A. Sellitto, “Phonon hydrodynamics and phonon-boundary scattering in nanosystems,” *J. Appl. Phys.*, vol. 105, no. 1, p. 014317, 2009.
- [43] P. Tabeling, *Introduction To Microfluidics*, Oxford, Oxford University Press, 2005.
- [44] H. Bruus, *Theoretical Microfluidics*, Oxford, Oxford University Press, 2007.
- [45] M. Morishita, T. Kuroda, A. Sawada, and T. Satoh, “Mean free path effects in superfluid He^4 ,” *J. Low Temp. Phys.*, vol. 76, pp. 387–415, 1989.

- [46] L. Galantucci, C. F. Barenghi, M. Sciacca, M. Quadrio, and P. Luchini, "Turbulent superfluid profiles in a counterflow channel," *J. Low Temp. Phys.*, vol. 162, pp. 354–360, 2011.
- [47] W. Vinen, "Mutual friction in a heat current in liquid helium II. III. Theory of the mutual friction," *Proc. R. Soc. London, A*, vol. 240, no. 1231, pp. 493–515, 1957.
- [48] K. W. Schwarz, "Three-dimensional vortex dynamics in superfluid He 4: homogeneous superfluid turbulence," *Phys. Rev. B*, vol. 38, no. 4, pp. 2398–2417, 1988.
- [49] C. Barenghi, R. Donnelly, and W. Vinen, "Friction on quantized vortices in helium II. A review," *J. Low Temp. Phys.*, vol. 52, nos. 3–4, pp. 189–247, 1983.
- [50] L. Galantucci and M. Sciacca, "Turbulent superfluid profiles and vortex density waves in a counterflow channel," *Acta Appl. Math.*, vol. 122, no. 1, pp. 407–418, 2012.
- [51] L. Galantucci and M. Sciacca, "Non-classical velocity statistics in counterflow quantum turbulence," *Acta Appl. Math.*, vol. 132, pp. 273–281, 2014.
- [52] H. Hall and W. Vinen, "The rotation of liquid helium II. II. The theory of mutual friction in uniformly rotating helium II," *Proc. R. Soc. London Ser. A: Math. Phys. Sci.*, vol. 238, no. 1213, pp. 215–234, 1956.
- [53] R. Keys, "Cubic convolution interpolation for digital image processing," *IEEE Trans. Acoust., Speech, Signal Process.*, vol. 29, no. 6, pp. 1153–1160, 1981.
- [54] D. Jou, M. Mongioli, and M. Sciacca, "Hydrodynamic equations of anisotropic, polarized and inhomogeneous superfluid vortex tangles," *Phys. D*, vol. 240, no. 3, pp. 249–258, 2011.
- [55] T. Lipniacki, "Dynamics of superfluid 4He: two-scale approach," *Eur. J. Mech. B Fluids*, vol. 25, no. 4, pp. 435–458, 2006.
- [56] D. Jou, M. Sciacca, and M. S. Mongioli, "Vortex dynamics in rotating counterflow and plane Couette and Poiseuille turbulence in superfluid helium," *Phys. Rev. B*, vol. 78, no. 12, p. 024524, 2008.
- [57] D. Jou and M. Mongioli, "Description and evolution of anisotropy in superfluid vortex tangles with counterflow and rotation," *Phys. Rev. B*, vol. 74, no. 11, p. 054509, 2006.
- [58] C. F. Barenghi, S. Hulton, and D. C. Samuels, "Polarization of superfluid turbulence," *Phys. Rev. B*, vol. 134, no. 4, p. 275301, 2002.